INDONESIAN SCHOLAR SOCIETY

Indones. J. Chem. Stud.
2023, 2(1), 13–21
Available online at journal.solusiriset.com
e-ISSN: 2830-7658; p-ISSN: 2830-778X

Indonesian Journal of Chemical Studies

Magnetically Separable Humic Acid-Chitin Based Adsorbent as Pb(II) Uptake in Synthetic Wastewater

Ngatijo[1], Lenny Marlinda[1], Wukhoidatul Malihah[1], Bayu Ishartono[2], Rahmat Basuki*[3]

[1]*Department of Chemistry, Faculty of Science and Technology, Universitas Jambi, Jambi, Indonesia*

[2]*Doctoral Program, Department of Chemistry, Universitas Gadjah Mada, Yogyakarta, Indonesia*

[3]*Department of Chemistry, Republic of Indonesia Defense University, Bogor, Indonesia*

Received: 23 Feb 2023; Revised: 5 Apr 2023; Accepted: 25 Apr 2023;
Published online: 7 May 2023; Published regularly: 30 Jun 2023

***Abstract*—**Modification of humic acid (HA) from the peat soil of Jambi province, Indonesia with chitin and magnetite to form Fe_3O_4/HA-chitin has been successfully carried out. The successful synthesis was identified from characterization with functional group analysis, crystal analysis, magnetic strength measurement, and morphological and elemental analysis. The application of Fe_3O_4/HA-chitin to adsorb Pb(II) ion was analyzed using the Lagergren, Ho, Santosa, and RBS kinetics models (kinetics study) and the Langmuir, Freundlich, Dubinin-Radushkevich (DR), and Temkin isotherm model (isotherm study). The kinetics study followed the Ho model (pseudo-second order) with R^2 and k_{Ho} of 0.9997 and 10264.59 g/mol min, respectively. The results of the data applicable to the Freundlich model showed that several sites were capable of multilayer adsorption (B) with a large enough adsorption capacity of 929.19 mg/g (about 28 times higher than the monolayer adsorption of Langmuir data). However, the outermost layer had a feeble adsorption energy of 0.51 kJ/mol, as measured by Temkin's adsorption energy. In the layer between the first layer (Langmuir) and the outermost layer (Freundlich), the DR isotherm was measured at a capacity of 104.87 mg/g (q_D, the 3rd layer of the first layer) the adsorption energy was measured at 12.91 kJ/mol. A cross-study on the prediction of adsorption energy using the Santosa and RBS kinetics models showed that the RBS model had an adsorption energy value (26.45 kJ/mol) that was closer to the adsorption energy value of the Langmuir isotherm (27.55 kJ/mol).

***Keywords*—** Adsorption; Fe_3O_4/HA-Chitin; Humic acid; Pb(II) uptake.

1. INTRODUCTION

Lead is a non-ferrous heavy metal widely used in chemical industries, including batteries, paints, pesticides, detergents, and other chemicals [1]. However, Pb(II), in chemical industry wastewater, poses a crucial threat to the environment and human health. Pb(II) is a toxic heavy metal that can accumulate in the food chain because it cannot be degraded by microorganisms [2-3]. In humans, it can cause critical problems with blood circulation, digestion, and reproduction [4]. As a result, serious efforts to remove the presence of Pb(II) in wastewater are required. Precipitation [5-6], evaporation [7], membrane separation [8-9], and electrochemical [10-11] are some methods developed and used to remove Pb(II). Unfortunately, several of these technologies have many drawbacks, including high costs, low efficiency, and potential for secondary environmental impact. Thus, it is critical to employ more environmentally friendly alternatives.

The adsorption method is a simple, efficient, and highly effective method for removing heavy metal ions from water [12-13]. The adsorption method's mechanism usually involves physical and chemical interactions on the adsorbent's surface with the adsorbate resulting in a decrease in the adsorbate's concentration. The use of biochar [3,14], mesoporous silica and its modifications [15-16], and cellulose and other organic polymers [8,11,14,17] as adsorbents to remove the presence of Pb(II) in wastewater has been widely reported. Peatlands with a relatively high content of humic acid (HA), which can be used as an adsorbent, are one of the abundant natural resources available in Jambi province, Sumatera, Indonesia.

HA compounds are macromolecules with the functional groups –COOH and –OH alcoholates, as well as phenolics, which can interact with ionic metals. Due to this interaction ability, HA has been used as an adsorbent for heavy metal ions of Cd(II) and Pb(II), with adsorption results of 60.2% and 81.6%, respectively [18].

***Corresponding author**.
Email address: rhmtbsq@gmail.com
DOI: 10.55749/ijcs.v2i1.22

However, the use of HA as an adsorbent directly has a weakness in that the HA adsorbent is stable under acidic conditions (pH = 3) but dissolves in a pH > 6, reaching up to 95% [17]. The occurrence of HA dissolution has prompted researchers to start working on ways to improve the efficiency of this adsorbent by modifying it with chitin [19-20].

Chitin is selected because it can withstand a wider range of medium acidity. It acts as a molecular buffer, improving the structure of HA and allowing it to survive at alkaline pH levels [21]. Furthermore, the presence of acetamide groups derived from chitin increases the number of HA active sites. This group will act as a metal ion exchanger, increasing the ability to adsorb metal cations. The difficulty of separating the adsorbent from the processed solution is still a problem when using HA-chitin as an adsorbent. Physical separation techniques such as centrifugation and filtration necessitate a significant investment in time, energy, and effort. As a result, alternative adsorbents must be developed that can be easily separated from the adsorption medium using a simple process.

2. EXPERIMENTAL SECTION

2.1. Materials

All reagents were manufactured in analytical grades from Merck Co. Inc. (Germany) and used without further purification, including $Pb(NO_3)_2$, HCl 37%, HNO_3, NaOH, $FeCl_3 \cdot 6H_2O$, $FeSO_4 \cdot 7H_2O$, NH_4OH 25%, and NaOCl 0.315%. Peat soil as a source of HA provided from Muaro Jambi Regency, Jambi Province, Sumatra. Chitin was isolated from crab shells waste. A set of laboratory glassware, Memmert oven, Mettler AE100 analytical balance, 80 mesh Fischer sieve, burette, and stand, Mettler Toledo pH meter, reflux apparatus, IKA C-MAG HS 4 magnetic stirrer, shaker, Nabertherm furnace, and Hettich EBA 270 centrifuge were among the preparation tools utilized in this investigation.

2.2. Characterization

The identification of some functional groups of Fe_3O_4/HA-chitin materials was accomplished by pelletizing the samples with potassium bromide (KBr) powder and analyzing them with a Shimadzu Prestige 21 Fourier Transform Infrared Spectrometer (FTIR) in the 400-4000 cm^{-1} range. A Phillips PANalytical XPert MPD was used to create Fe_3O_4/HA-chitin materials X-ray diffraction (XRD) patterns. From 5.00° to 59.98° (2θ), diffraction patterns were obtained with a step size of 0.02. The surface area and pore diameter of the adsorbent was measured with nitrogen gas at 77K using the Quantachrome Quadrasorb-Evo Surface Area & Pore Size Analyzer instrument. A Vibrating Sample Magnetometer Oxford 1.2H instrument was used to measure the magnetic properties of Fe_3O_4/HA-chitin for 20 min at a magnetic field change rate of 0.25 T/min. A Scanning Electron Microscope-Energy Dispersive X-Ray (SEM-EDX) Phenom Desktop ProXL was used to analyze the surface morphology and chemical element properties of the composite.

2.3. Extraction and purification of HA

The steps for extracting HA were carried out using a modified method from a previous study [21]. To begin the extraction, 500 g of dry peat soil was mixed with 5 L of NaOH 0.1 M. The resulting suspension was shaken for 24 h at room temperature. The alkaline supernatant was separated from the residue by centrifugation, then acidified to pH 1 with 6 M HCl and stored at room temperature for 24 h. Centrifugation was used to separate the supernatants (fulvic acid/FA) from the coagulants (HA). The coagulants were dried in an oven at 60 °C. The obtained HA was analyzed for ash content and moisture content, and its functional groups were characterized using FTIR.

2.4. Isolation and characterization of chitin

The stages of isolation and characterization of chitin from crab shells were carried out by following a modified method from a previous study [21]. Finely ground dried crab shells were sieved through an 80 mesh sieve. The crab shell powder was demineralized by soaking it in 1 M HCl at a ratio of 1:15 (w/v), stirring it for 1 h at 75 °C, and filtering it. The residue was washed with distilled water until the pH was neutral, then dried for 4 h in a 100 °C oven.

The demineralized powder was deproteinized by dissolving it in a NaOH 3.5% (w/w) at a ratio of 1:10 (w/v), refluxing for 2 h at 65 °C, and filtering the results. The deproteinized residue was washed with distilled water until the pH reached neutral, then dried at 60 °C. The depigmentation step was completed by bleaching the deproteinized powder for 30 min at room temperature with 0.315 percent NaOCl at a 1:10 (w/v) ratio. The suspension was washed with distilled water and dried at 60 °C. FTIR was used to analyze the final result.

2.5. Immobilization of HA on chitin

The HA-chitin composite was synthesized by reacting 30 g of chitin in 200 mL of 0.5 M HCl and 4 g of HA in 500 mL of 0.5 M NaOH. A total of 200 mL of activated HA solution was mixed with 200 mL of activated chitin gel solution and stirred continuously for 24 h. The mixture was filtered and the precipitation was washed using distilled water to dry in an oven at 50-60 °C for 30 min. The results were characterized using FTIR and SEM-EDX.

2.6. Synthesis of Fe_3O_4/HA-chitin composite

Using the co-precipitation method, Fe_3O_4/HA-chitin adsorbent material was prepared. 1.52 g $FeCl_3 \cdot 6H_2O$ and 1.05 g $FeSO_4 \cdot 7H_2O$ were dissolved in 25 mL distilled water and stirred for 30 min at 90 °C. A 25% NH_4OH solution was added simultaneously with 25 mg HA-chitin composite material which was added quickly.

Stirring temperatures were kept at 90 °C for 30 min before cooling down to room temperature. The black sediment was removed from the solution and washed with distilled water until the pH was balanced. The precipitate was neutralized and dried at 60 °C before being characterized with FTIR, XRD, VSM, BET, and SEM-EDX

2.7. Sorption study of Pb(II)

2.7.1. Kinetics study

Twenty mL of 10 mg/L (pH= 5.00) Pb(II) solution was contacted with 20±1 mg Fe_3O_4/HA-chitin. The mixture was shaken for 10 min. The mixture was then separated by an external magnet. The remaining Pb(II) in the filtrate was measured with AAS. The difference between the initial Pb(II) concentration and remaining Pb(II) in the filtrate was recorded by the adsorbed Pb(II) on the Fe_3O_4/HA-chitin. A similar procedure was also performed at different contact times: 30, 60, and 120 min.

2.7.2. Isotherm study

Twenty mL of 10 mg/L Pb(II) solution was contacted with 20±1 mg Fe_3O_4/HA-chitin. The mixture was shaken for 3 h until equilibrium was reached. The mixture was then separated by an external magnet. The remaining Pb(II) in the filtrate was measured with AAS. The difference between the initial Pb(II) concentration and the remaining Pb(II) in the filtrate was recorded by the adsorbed Pb(II) on the Fe_3O_4/HA-chitin. A similar procedure was also performed at different Pb(II) concentrations: 20, 30, 40, 60, 80, and 100 mg/L.

3. RESULT AND DISCUSSION

3.1. Extraction and purification of HA

The extraction and purification of HA from peat soil were conducted according to the International Humic Substance Society's procedures (IHSS). Since humic compounds (HA and FA) are soluble in bases, while humin and other non-humate compounds are not, the extraction of humic compounds is based on the displacement of components from the original material into the NaOH solution. The use of NaOH solution causes OH^- ions to interact strongly with H^+ ions from humic compounds, allowing for proper extraction of the components according to Equation 1 [22]:

$$R\text{–}O^- Na^+ + CO_2 \rightarrow HO\text{–}R\text{–}CO_2Na^+ \quad (1)$$

After the extraction process is complete, the HA is purified to remove any impurities present during the extraction stage. The purification process was carried out by adding 6 M HCl to the solution to separate the HA and FA. This completely precipitates HA by forming hydrogen bonds between HA and H^+ ions. Therefore, the functional groups in HA are difficult to deproteinize, resulting in aggregates or clumps characterized by HA deposits.

The ash and water contents of HA obtained during the extraction and purification process were determined. The ash and moisture contents of the peat soil samples were 64.67% and 28.11%, respectively, before extraction and purification. The ash and water contents of the HA samples were 21.47% and 11.88%, respectively, after the extraction and purification process. The difference in values indicates that metal oxides in the peat soil sample are significantly reduced during the HA extraction and purification processes.

3.2. Isolation and characterization of chitin

Demineralization, deproteination, and depigmentation processes were used in this study to isolate chitin from crab shells. The demineralization process removes inorganic compounds from the crab shells in the form of mineral components. Crab powder samples can be immersed in a 1:15 (w/v) solution of 1 M HCl to remove the mineral content. The use of an HCl solution is intended to cause minerals (inorganic compounds in the form of salts) to react with HCl to form a soluble chloride salt, resulting in a chitin precipitate, as shown in reaction Equation 2-6 [23]:

$$CaCO_{3(s)} + 2HCl_{(aq)} \rightarrow CaCl_{2(aq)} + H_2O_{(l)} + CO_{2(g)} \quad (2)$$

$$Ca_3(PO_4)_{2(s)} + 6HCl_{(aq)} \rightarrow 3CaCl_{2(aq)} + 2H_3PO_{4(aq)} \quad (3)$$

$$Na_2CO_{3(aq)} + 2HCl_{(aq)} \rightarrow 2NaCl_{(aq)} + H_2O_{(l)} + CO_{2(g)} \quad (4)$$

$$MgCO_{3(s)} + 2HCl_{(aq)} \rightarrow MgCl_{2(aq)} + H_2O_{(l)} + CO_{2(g)} \quad (5)$$

$$H_2CO_{3(g)} \rightarrow H_2O_{(l)} + CO_{2(g)} \quad (6)$$

Deproteination is the process of separating or releasing protein bonds from chitin. The crude chitin content from the demineralization process was reacted with 3.5% (w/v) NaOH in reflux for 2 h at a ratio of 1:10 (w/v). According to the reaction Equation 7-11, the use of NaOH aims to dissolve physically bound proteins (meat residues that are still attached) or those that are covalently bound to the chitin functional group [24]:

$$C_6H_{12}N_2O_3 + 2NaOH \rightarrow 2C_3H_6NNaO_2 + H_2O \quad (7)$$

$$C_{10}H_{16}N_2O_7 + 2NaOH \rightarrow 2C_5H_8NNaO_4 + H_2O \quad (8)$$

$$C_{18}H_{20}N_2O_3 + 2NaOH \rightarrow 2C_9H_{10}NNaO_2 + H_2O \quad (9)$$

$$C_{10}H_{20}N_2O_3 + 2NaOH \rightarrow 2C_9H_{10}NNaO_2 + H_2O \quad (10)$$

$$C_{12}H_{26}N_4O_3 + 2NaOH \rightarrow 2C_6H_{13}N_2NaO_2 + H_2O \quad (11)$$

The reddish pigment in chitin was removed during the depigmentation stage. This astaxanthin dye can be removed by depigmentation with NaOCl solution, which gives the chitin product to obtain a more appealing appearance. This is possible because NaOCl is a strong oxidizing agent that can oxidize the color pigments in the crab shells. At this point, the deproteinized sample was dissolved in 0.315% NaOCl at a 1:10 (w/v) ratio. Two phases are formed during this process: a white solid phase (chitin) and a yellowish-orange liquid phase (astaxanthin). The yellowish-orange color in the liquid

phase indicates that NaOCl interacts with the color pigments present in chitin. The colored pigments combine with Na^+ ions to form complex compounds, while ClO^- ions bind to the chitin polymer chains. Color pigments are bound by Na^+ ions, which weaken the hydrogen bonds that exist between astaxanthin and chitin, allowing them to be separated easily from chitin.

3.3. Characterization of Fe_3O_4/HA-chitin composite

FTIR spectra analysis provides information about the functional groups of the synthesized products, as shown in **Fig. 1**. Based on the analysis of the HA infrared spectra in **Fig. 1a**, the absorption at 3448 cm^{-1} denotes the –OH stretching vibrations of the successfully synthesized HA compound. The aliphatic C–H stretching vibrations in HA was indicated by the absorption at 2904 and 2854 cm^{-1}. The absorption band around 1705 cm^{-1} depicted the stretching vibration of C=O from the –COOH group. In accordance with previous studies, the absorption band at 1627 cm^{-1} was interpreted as –C=C aromatic or C=O (conjugated ketones) bound to the H atom [25]. In agreement with previous investigations, the –OH bending vibrations and the C=O stretching vibrations of –COOH were detected by the emergence of absorption at 1273 cm^{-1} [26].

The infrared spectra of chitin isolated from crab shells are shown in **Fig. 1b**. The stretching vibration of –OH was detected at 3448 cm^{-1}. The symmetric stretching of aliphatic C–H bonds was indicated by the absorption at 2925 and 2855 cm^{-1}. C=O absorption in the $-NHCOCH_3$ group could be seen at 1658 cm^{-1}, while N-H bending vibrations at 1558 cm^{-1} [21]. The absorption band characteristic of the amide group (N–H stretching) does not appear at 3270 and 3100 cm^{-1} due to overlapping with neighboring absorption bands (stretching O-H). It appeared as an absorption band at 1658-1558 cm^{-1} as N–H bending. This absorption non-sharpness bands are due to overlapping with neighboring absorption bands. The C–O strain is responsible for another bond, which is discovered at 1072 cm^{-1}.

The N-H stretching appeared at 3500-3300 cm^{-1}. This absorption band of N-H stretching does not appear due to overlapping with neighboring absorption bands (stretching O-H). So, for confirmation, we had seen at 1658-1558 cm^{-1} as the N-H bending.

Fig. 1c shows the results of the FTIR spectra of the synthesized Fe_3O_4 from this study. The stretching and bending vibrations of the –OH group were indicated by the absorption bands at 3425 and 1635 cm^{-1}, respectively. Absorption bands at 586 and 624 cm^{-1} were assigned to a strain in the Fe-O bond [27]. **Fig. 1d** explains that according to previous studies, the absorption bands at 1566 and 1658 cm^{-1} were designated for the presence of HA in the adsorbent, while the absorption band at 1157 cm^{-1} referred to a new C-O-C group.

Fig. 1e shows the FTIR spectra of Fe_3O_4/HA-chitin obtained in this study. The absorption peak at 3410 cm^{-1}, was designated to the stretching vibration of the –OH group bound to Fe–OH, followed by the appearance of an absorption band at 1600 cm^{-1}, indicating a stretching vibration –COO. Absorption at 1558 cm^{-1} was assigned the C=O vibration of Fe_3O_4 with HA [28]. The presence of stretching vibrations from the Fe–O bond was indicated by the absorption band at 586 cm^{-1} [27]. The presence of multiple absorption bands suggests that the carboxylate group in HA is critical to ligand exchange bonding between HA-chitin and the Fe_3O_4 surface.

The purpose of XRD characterization is to learn more about a material's crystal structure and compound

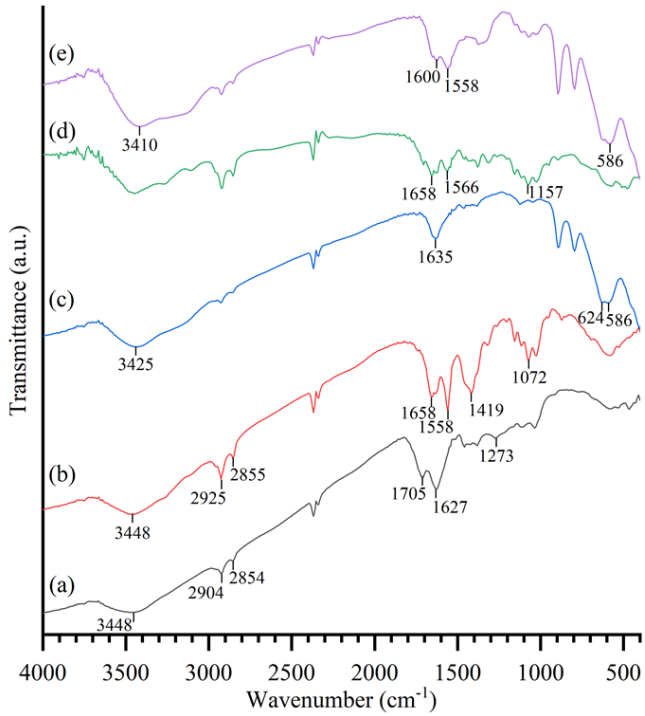

Fig. 1. Infrared spectra of (a) HA; (b) chitin; (c) Fe_3O_4; (d) HA-chitin; and (e) Fe_3O_4/HA-chitin.

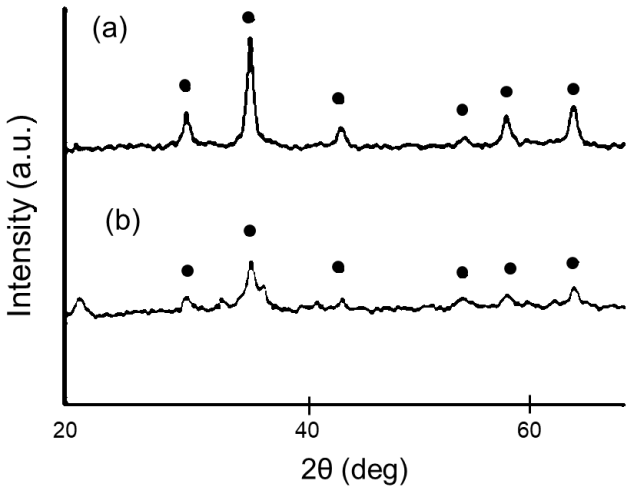

Fig. 2. Diffraction patterns of (a) Fe_3O_4 and (b) Fe_3O_4/HA-chitin (black circle indicating characteristic peak of Fe_3O_4 cubic structure).

composition. The diffraction peaks in the 15°–80° range were used to interpret the X-ray diffraction pattern of Fe_3O_4 in **Fig. 2a**. In accordance with JCPDS No. 19-0629, the diffraction pattern of Fe_3O_4 showed several high peaks at angles of 2θ (marked with a black circle in **Fig. 2**) at 30.25°; 35.64°; 43.92°; 53.70°; 57.22°; and 62.90° indicating a cubic structure [29]. **Fig. 2b** shows the appearance of peaks at several angles 2θ = 30.25°; 35.64°; 43.92°; 53.70°; 57.22°; and 62.90° in the diffraction pattern of Fe_3O_4/HA-chitin as a new adsorbent. This indicates that the adsorbent formed after coating Fe_3O_4 with AH-chitin does not affect on the crystal structure of the metal. The appearance of this diffraction pattern supports the data from the FTIR spectrum at 586 cm^{-1}, which shows the stretching vibration of the adsorbent Fe–O bond and proves that HA-chitin contains Fe_3O_4.

The VSM analysis can be used to determine the magnetic properties of the synthesized Fe_3O_4/HA-chitin adsorbent. The hysteresis curve in **Fig. 3** compares the degree of magnetism (M) of Fe_3O_4 (a) and Fe_3O_4/HA-chitin (b). The existence of the magnetization value is linked to the magnetic properties of Fe_3O_4's main function, acting as an intermediary in the separation process using an external magnet. In this study, Fe_3O_4 without HA-chitin coating had a higher magnetization value (37.39 emu/g) than Fe_3O_4 with HA-chitin (29.17 emu/g). Based on these findings, it can be concluded that HA-chitin has coated Fe_3O_4, as evidenced by a magnetization value of 29.17 emu/g. This has a significant impact on Fe_3O_4's magnetic properties. This reduction, however, is still effective as a magnetic field separation characterized by the ability of the adsorbent to be attracted by the previously tested external magnetic field.

Nitrogen gas adsorption can be used to determine the material's surface area and pore diameter. Analysis of a material's surface area and pore diameter used the

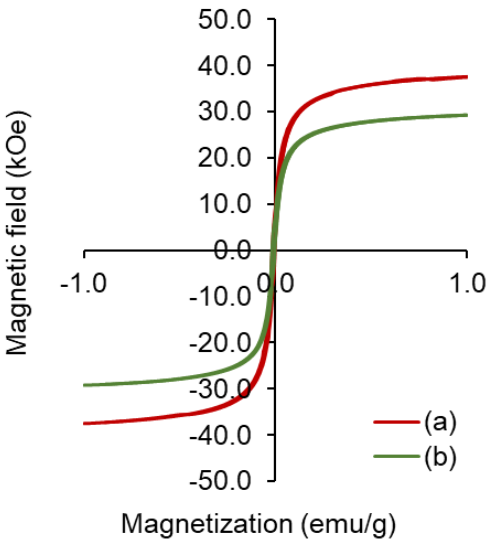

Fig. 3. The VSM hysteresis curve of (a) Fe_3O_4 and (b) Fe_3O_4/HA-chitin.

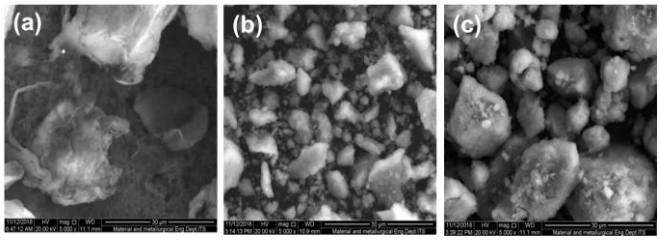

Fig 4. Surface morphology of (a) HA-chitin; (b) Fe_3O_4; and (c) Fe_3O_4/HA-chitin with 5000 times magnitude.

Brunauer-Emmett-Teller (BET) and Barrett-Joyner-Halenda (BJH) methods, respectively. Adsorbents have important properties, such as surface area, particle size, and pore diameter. The adsorbent synthesis of Fe_3O_4 with HA-chitin had a surface area of 69.366 m^2/g, an average particle diameter of 27.54 nm, and a pore diameter of 191 Å. Based on these findings, it can be concluded that HA-chitin coating Fe_3O_4 can increase the surface area and average particle diameter, resulting in a higher adsorption capacity for the adsorbent formed. Further, the mechanism of Fe_3O_4 formation was described using this chemical reaction (Equation 12) [30].

$$2Fe^{3+} + Fe^{2+} + 8OH^- \rightarrow Fe_3O_4 + 4H_2O \quad (12)$$

Magnetite precipitated immediately after being introduced in a highly alkaline solution. Typically, this produces tiny nanoparticles with a diameter of 20 nm or less that are endowed with superparamagnetic properties because of the magnetic domain's constrained size. Furthermore, the formation of nanometer sized particles indicates that the adsorbent has been synthesized as expected using the coprecipitation method with a precipitating agent in the form of NH_4OH.

The SEM-EDX characterization sees the surface morphology and then determines the component or elemental composition of the synthesized sorbent. **Fig. 4a** shows the surface morphology of HA-chitin, which looks like sheets or layers with fine fiber content. This finding is consistent with previous studies [31].

The surface morphology of Fe_3O_4 in **Fig. 4b** had a non-uniform particle shape but was generally round and pointed. The morphology of the Fe_3O_4/HA-chitin

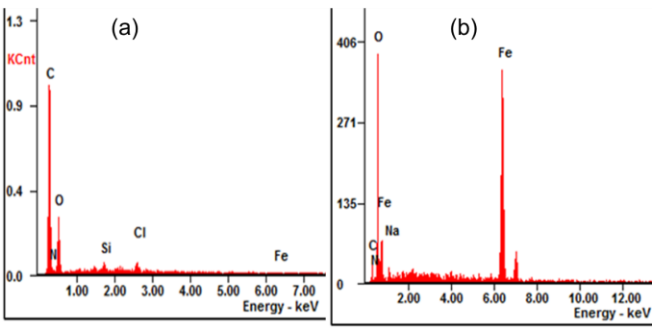

Fig. 5. Elemental analysis obtained from EDX of (a) HA-chitin; and (b) Fe_3O_4/HA-chitin.

adsorbent in **Fig. 4c** showed a non-uniform shape of the adsorbent's surface morphology. This is due to the presence of HA-chitin, which coats Fe_3O_4, resulting in a larger fractal size (**Fig. 4c**) compared to Fe_3O_4 (**Fig. 4a**). This is owing to the Fe_3O_4 surface's combination of coating agent (HA), suggesting that the Fe_3O_4 surface's AH-chitin coating is successful.

The results of the EDX analysis show the composition of the elements contained in the adsorbent material and the success of the Fe_3O_4/HA-chitin adsorbent preparation. **Fig. 5** depicts the characterization of the elemental composition because of the EDX analysis for each material, which corresponds to the composition of the elements synthesized. The composition of the elements **Fig. 5a** shows that C (53.40%), N (6.08%), O (35.92%), Si (0.89%), Cl (0.98%), and Fe (0.06%) are still present in HA-chitin. The presence of Fe (67.29%), O (26.30%), and C (6.41%) elements were detected in the EDX Fe_3O_4/HA-chitin results (**Fig. 5b**). **Fig. 5** shows that the Fe_3O_4 was successfully coated using HA-chitin, according to several elements discovered using the EDX instrument.

3.4. Kinectics study

Investigation of adsorption kinetics was carried out using the application of time variation on linear models from Lagergren (Equation 13), Ho (Equation 14), Santosa (Equation 15) [32], and Rusdiarso-Basuki-Santosa/RBS (Equation 16) [33-34].

$$\ln(q_e - q_t) = \ln q_e - k_{Lag} t \quad (13)$$

$$\frac{t}{q_t} = \frac{1}{k_{Ho}\left(q_e^{\,2}\right)} + \frac{1}{q_e} t \quad (14)$$

$$\frac{1}{C_0 - Xq_e} \ln\left(\frac{q_e(C_0 - Xq_t)}{C_0(q_e - q_t)}\right) = k_s t \quad (15)$$

$$\ln\left(\frac{C_0 C_b - x_e x}{x_e - x}\right) = k_a \left(\frac{C_0 C_b - x_e^{\,2}}{x_e}\right) t - \ln\left(\frac{x_e}{C_0 C_b}\right) \quad (16)$$

The application of kinetic data in equations (13)-(16) is presented in **Fig. 6a-6d**. The model that best represents the kinetic system of this study based on its linearity was the Ho kinetic model, with an R^2 of 0.9997 (**Table 1**). The parameters resulting from the kinetics of Ho were the adsorption rate constant (k_{Ho}) of 10264.59 L/mol min and the adsorbed Pb(II) at equilibrium (q_e) of 3.57×10^{-5} mol/g.

Although it has the best linearity, the Ho kinetic model has several weaknesses, namely the resulting parameters are very minimal for cross-study with other parameters, for example, the adsorption isotherm parameter. The parameters generated from the kinetics of Ho were the calculated k_{Ho} and q_e. Meanwhile, for cross-study adsorption isotherm parameters, the kinetic model must produce a desorption rate constant (k_{des}). Through the relationship of the adsorption equilibrium constant, K, that $K=k_a/k_d$, a cross-study between the kinetic parameters and the adsorption isotherm can be carried out. However, the only thing that can be compared from the parameter Ho is the calculated result of q_e with the experimental q_e. Comparison of the calculated results of q_e (3.66×10^{-5} mol/g) and the experimental results of qe (3.57×10^{-5} mol/g) in this study has very close values, which confirms that adsorption follows the model Ho kinetics.

Santosa [32] and Rusdiarso et al. [33-34] develop a kinetic model that produces a *k* desorption parameter (k_d), which can be compared with the adsorption isotherm parameter, K, through the $k_a/k_d=K$ relationship so that a cross-study can be carried out whether the kinetic parameters describe the original value. The results of the application of the kinetic data of this study to the Santosa model showed a fairly good R^2 value (0.9929) with the adsorption rate constants (k_S) and desorption (k_{dS}) respectively of 2105.50 L/mol min and 1.05×10^{-4} min^{-1}. The desorption rate constant (k^{dS}) for the Santosa model is obtained from the plot ln (1-{q_t/q_e}) versus t (the plot not shown) with the slope being a function of $k_S.C_0+k_{dS}$. Using the adsorption energy formula, $E_S = -RT \ln K_S$ where K_S is k_S/k_{dS}, it is obtained E_S = 40.73 kJ/mol. The E_S value is quite far from the E_L value from Langmuir. Thus, it can be concluded that the k_S and k_{dS} values do not reflect the adsorption of Pb(II) on Fe_3O_4/HA-chitin.

The linearity (R^2) of the application of time variation data in the RBS kinetics model was also quite good (0.9967). The parameters resulting from the RBS model were k_a = 742.96 L/mol min, k_d = 0.01714 min^{-1}, and calculation q_e = 3.80×10^{-5} mol/g. Using the same calculation as E_S, the E_{RBS} value = 26.45 kJ/mol, where this E_{RBS} value was very close to the E value of Langmuir (26.31 kJ/mol). In addition, the comparison of

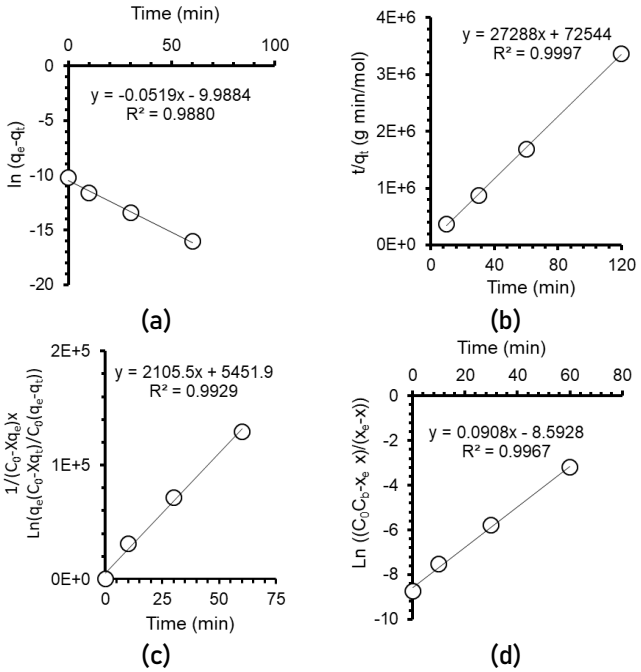

Fig. 6. Linear plot of (a) Lagergren, (b) Ho, (c) Santosa, and (d) RBS kinetics models.

Table 1. Kinetics parameter of Lagergren, Ho, Santosa, and RBS kinectics models.

Kinetics Models	Kinetics Parameters	value
Lagergren	R^2	0.9880
	k_{Lag} (min^{-1})	0.0519
Ho	R^2	0.9997
	k_{Ho} (L/min mol)	10264.59
Santosa	R^2	0.9929
	k_s (L/mol min)	2105.50
	k_{ds} (min^{-1})	1.05×10^{-4}
	K_s (L/mol)	1.38×10^{7}
RBS	R^2	0.9967
	k_a (L/mol min)	742.96
	k_d (min^{-1})	0.01714
	k_a/k_d (L/mol)	43336.72

the calculated value of q_e from the RBS kinetics model (3.80×10^{-5} mol/g) and the experimental results of q_e (3.57×10^{-5} mol/g) in this study had a fairly close value. From the analysis results, it can be concluded that the RBS kinetics model is relatively suitable for describing the adsorption of Pb(II) on Fe_3O_4/HA-chitin and can be used to predict the adsorption energy merely from kinetic data.

3.5. Thermodynamic study

The adsorption isotherm parameters were generated from the application of experimental data of concentration variations in a linear model of Langmuir (Equation 17), Freundlich (Equation 18), Dubinin-Radushkevich, DR (Equation 19), and Temkin (Equation 20) isotherm models.

$$\frac{C_e}{q_e} = \frac{1}{K_L b} + \frac{1}{b} C_e \quad (17)$$

$$\ln q_e = \ln B + \frac{1}{n} \ln C_e \quad (18)$$

$$\ln q_e = \ln q_D - B_D \varepsilon^2 \quad (19)$$

$$q_e = \frac{RT}{b_T} \ln A_T + \frac{RT}{b_T} \ln C_e \quad (20)$$

The data application to the plot in Equations (17)-(20) is presented in **Fig. 7**. It can be seen that each model has a variable correlation coefficient (R^2), with the best R^2 obtained from the Freundlich model. Based on the Freundlich model, the adsorption capacity of Pb(II) on Fe_3O_4/HA-chitin was 32.52 mg/g with adsorption energy (E_L) of 27.55 kJ/mol (**Table 2**).

The magnitude of this adsorption energy indicates that the adsorption of Pb(II) on Fe_3O_4/HA-chitin occurs through physical interaction or ion exchange [34]. The fit of the isotherm data with the Freundlich isotherm model shows that Pb(II) is adsorbed and tends to be multilayer. Thus, it can be assumed that the site is possible to bind more than one Pb(II) ion.

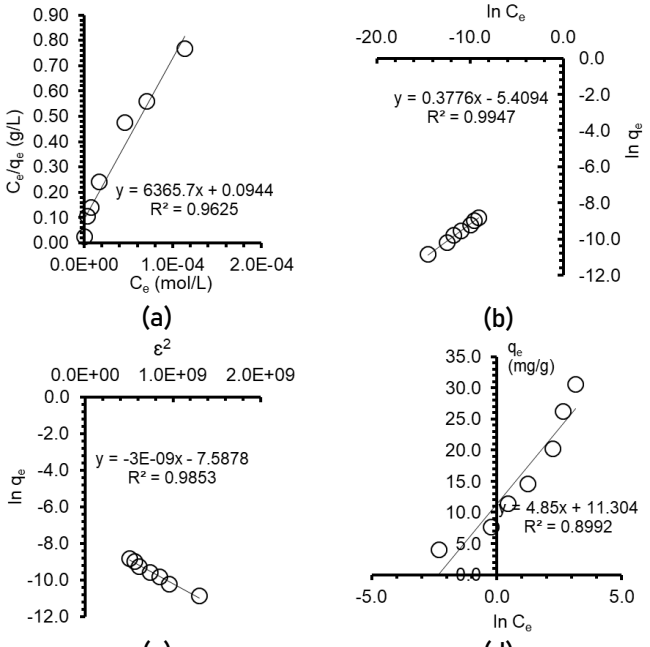

Fig. 7. Linear plot of (a) Langmuir, (b) Freundlich, (c) DR, and (d) Temkin isotherm models.

The results of applying the data to the Freundlich model show that there were several sites capable of multilayer adsorption (B) with a large enough adsorption capacity of 929.19 mg/g (about 28 times higher than of monolayer adsorption of Langmuir data). However, the outermost layer had very weak adsorption energy of 0.51 kJ/mol, as measured by Temkin's adsorption energy (**Table 2**).

In the layer between the first layer (Langmuir) and the outermost layer (Freundlich), the DR isotherm

Table 2. Isotherm parameters of Pb(II) sorption onto Fe_3O_4/HA-chitin

Isotherm Models	Isotherm Parameters	Value
Langmuir	b (mol/g; mg/g)	1.57×10^{-4} ; 32.52
	K_L (L/mol)	67425.85
	E_L (kJ/mol)	27.55
	R^2	0.9625
Freundlich	B (mol/g; mg/g)	4.47×10^{-3} ; 926.19
	n	2.96
	R^2	0.9947
D-R	q_D (mol/g; mg/g)	5.07×10^{-4} ; 104.87
	B_{D-R} (mol^2/J^2)	6.00×10^{-9}
	E_{D-R} (kJ/mol)	12.91
	R^2	0.9853
Temkin	A_T (L/g)	10.26
	b_T (J/mol)	510.84
	R^2	0.8992

was measured at a capacity of 104.87 mg/g (q_D, the 3rd layer of the first layer) the adsorption energy was measured at 12.91 kJ/mol. These results provide the fact that the outer layer of Pb(II) adsorbed on Fe_3O_4/HA-chitin, lowered the adsorption energy.

CONCLUSION

Modification of HA from the peat soil of Jambi province with chitin and magnetite to form Fe_3O_4/HA-chitin had been successfully carried out. The success synthesis was identified from characterization with FTIR, XRD, VSM, and SEM-EDX. Fe_3O_4/HA-chitin was then applied to adsorb Pb(II) ions from the solution. The Pb(II) adsorption followed the Freundlich isotherm (R^2= 0.9947), showing that the adsorption occurred in the multilayer with an adsorption capacity of 926.19 mg/g. For the monolayer Langmuir model, the R^2 was 0.9625 with an adsorption capacity of 32.52 mg/g. The kinetic study followed the Ho model (pseudo-second order) with R^2 and k_{Ho} of 0.9997 and 10264.59 g/mol min, respectively. A cross-study on the prediction of adsorption energy using the Santosa and RBS kinetics models showed that the RBS model had an adsorption energy value (26.45 kJ/mol) that was closer to the adsorption energy value of the Langmuir isotherm (27.55 kJ/mol)

SUPPORTING INFORMATION

There is no supporting information of this paper. The data that support the findings of this study are available on request from the corresponding author (RB).

ACKNOWLEDGEMENTS

Ngatijo is grateful to Jambi University for partly providing financial support through the Peat Research scheme (Contract No: 453/UN21.18/PG/SPK/2020). RB acknowledges The Republic of Indonesia Defense University for providing laboratory support

CONFLICT OF INTEREST

We declate that there is no conflict of interest in this paper among the authors.

AUTHOR CONTRIBUTIONS

N, LM, WM conducted the experiment; BI, RB, and N wrote and revised the manuscript. All authors agreed to the final version of this manuscript.

REFERENCES

[1] Ziegfeld, R.L. 1964. Importance and uses of lead. *Arch. Environ. Health*. 8(2). 202–212. doi: 10.1080/00039896.1964.10663657.

[2] Qin, D., Chen, A., Mamat, X., Li, Y., Hu, X., Wang, P., Cheng, H., Dong, Y., & Hu, G. 2019. Double-shelled yolk-shell Si@C microspheres based electrochemical sensor for determination of cadmium and lead ions. *Anal. Chim. Acta*. 1078. 32–41. doi: 10.1016/j.aca.2019.06.011.

[3] Wang, Y. & Liu, R. 2018. H2O2 treatment enhanced the heavy metals removal by manure biochar in aqueous solutions. *Sci. Total Environ.* 628–629. 1139–1148. doi: 10.1016/j.scitotenv.2018.02.137.

[4] Awual, M.R. & Hasan, M.M. 2014. Novel conjugate adsorbent for visual detection and removal of toxic lead(II) ions from water. *Microporous Mesoporous Mater.* 196. 261–269. doi: 10.1016/j.micromeso.2014.05.021.

[5] Rasaki, S.A., Thomas, T., & Yang, M. 2019. Co-precipitation strategy for engineering pH-tolerant and durable ZnO@MgO nanospheres for efficient, room-temperature, chemisorptive removal of Pb(II) from water. *J. Environ. Chem. Eng.* 7(2). 1-12. doi: 10.1016/j.jece.2019.103019.

[6] Cao, Y., Xiao, W., Shen, G., Ji, G., Zhang, Y., Gao, C., & Han, L. 2019. Carbonization and ball milling on the enhancement of Pb(II) adsorption by wheat straw: Competitive effects of ion exchange and precipitation. *Bioresour. Technol.* 273. 70–76. doi: 10.1016/j.biortech.2018.10.065.

[7] Hou, Q., Zhou, H., Zhang, W., Chang, Q., Yang, J., Xue, C., & Hu, S. 2021. Boosting adsorption of heavy metal ions in wastewater through solar-driven interfacial evaporation of chemically-treated carbonized wood. *Sci. Total Environ.* 759. 144317. doi: 10.1016/j.scitotenv.2020.144317.

[8] Roy Choudhury, P., Majumdar, S., Sahoo, G.C., Saha, S., & Mondal, P. 2018. High pressure ultrafiltration CuO/hydroxyethyl cellulose composite ceramic membrane for separation of Cr (VI) and Pb (II) from contaminated water. *Chem. Eng. J.* 336. 570–578. doi: 10.1016/j.cej.2017.12.062.

[9] Hoang, M.T., Pham, T.D., Verheyen, D., Nguyen, M.K., Pham, T.T., Zhu, J., & Van der Bruggen, B. 2020. Fabrication of thin film nanocomposite nanofiltration membrane incorporated with cellulose nanocrystals for removal of Cu(II) and Pb(II). *Chem. Eng. Sci.* 228. 115998. doi: 10.1016/j.ces.2020.115998.

[10] Zhang, J., Li, Y., Xie, X., Zhu, W., & Meng, X. 2019. Fate of adsorbed Pb(II) on graphene oxide under variable redox potential controlled by electrochemical method. *J. Hazard. Mater.* 367. 152–159. doi: 10.1016/j.jhazmat.2018.12.073.

[11] Ngana, B.N., Seumo, P.M.T., Sambang, L.M., Dedzo, G.K., Nanseu-Njiki, C.P., & Ngameni, E. 2021. Grafting of reactive dyes onto lignocellulosic material: Application for Pb(II) adsorption and electrochemical detection in aqueous solution. *J. Environ. Chem. Eng.* 9(1). 104984. doi: 10.1016/j.jece.2020.104984.

[12] Wang, Z., Xu, J., Yellezuome, D., & Liu, R. 2021. Effects of cotton straw-derived biochar under different pyrolysis conditions on Pb (II) adsorption properties in aqueous solutions. *J. Anal. Appl. Pyrolysis*. 157. 105214. doi: 10.1016/j.jaap.2021.105214.

[13] Ma, Y., Deng, Z., Li, Z., Lin, Q., Wu, Y., & Dou, W. 2021. Adsorption characteristics and mechanism for K2Ti4O9 whiskers removal of Pb(II), Cd(II), and Cu(II) cations in wastewater. *J. Environ. Chem. Eng.* 9(5). 106236. doi: 10.1016/j.jece.2021.106236.

[14] Qi, K., Lu, N., Zhang, S., Wang, W., Wang, Z., & Guan, J. 2021. Uptake of Pb(II) onto microplastic-associated biofilms in freshwater: Adsorption and combined toxicity in comparison to natural solid substrates. *J. Hazard. Mater.* 411. 125115. doi: 10.1016/j.jhazmat.2021.125115.

[15] Wang, W., Wu, G., Zhu, T., Yang, Y., & Zhang, Y. 2021. Synthesis of -thiazole Schiff base modified SBA-15 mesoporous silica for selective Pb(II) adsorption. *J. Taiwan Inst. Chem. Eng.* 125. 349–359. doi: 10.1016/j.jtice.2021.06.004.

[16] Nata, I.F., Wicakso, D.R., Mirwan, A., Irawan, C., Ramadhani, D., & Ursulla. 2020. Selective adsorption of Pb(II) ion on amine-rich functionalized rice husk magnetic nanoparticle biocomposites in aqueous solution. *J. Environ. Chem. Eng.* 8(5). 104339. doi: 10.1016/j.jece.2020.104339.

[17] Santosa, S.J., Siswanta, D., Kurniawan, A., & Rahmanto, W.H. 2007. Hybrid of chitin and humic acid as high performance sorbent for Ni(II). *Surf. Sci.* 601(22). 5155–5161. doi: 10.1016/j.susc.2007.04.163.

[18] Xu, H., Hu, X., Chen, Y., Li, Y., Zhang, R., Tang, C., & Hu, X. 2021. Cd(II) and Pb(II) absorbed on humic acid-iron-pillared bentonite: Kinetics, thermodynamics and mechanism of adsorption. *Colloids Surfaces A Physicochem. Eng. Asp.* 612. 126005. doi:

10.1016/j.colsurfa.2020.126005.

[19] Ngatijo, N., Basuki, R., Rusdiarso, B., & Nuryono, N. 2020. Sorption-desorption profile of Au (III) onto silica modified quaternary amines (SMQA) in gold mining effluent. *J. Environ. Chem. Eng.* 8(3). 103747. doi: 10.1016/j.jece.2020.103747.

[20] Basuki, R., Santosa, S.J., & Rusdiarso, B. 2017. The novel kinetics expression of Cadmium (II) removal using green adsorbent horse dung humic acid (Hd-Ha). *AIP Conf. Proc.* 1823(1). 020001. doi: 10.1063/1.4978074.

[21] Santosa, S.J., Siswanta, D., Sudiono, S., & Sehol, M. 2007. Synthesis and utilization of chitin-humic acid hybrid as sorbent for Cr(III). *Surf. Sci.* 601(22). 5148–5154. doi: 10.1016/j.susc.2007.04.161.

[22] Head, M.J. & Zhou, W.J. 2000. Evaluation of NaOH leaching techniques to extract humic acids from palaeosols. *Nucl. Instruments Methods Phys. Res. Sect. B Beam Interact. with Mater. Atoms*. 172(1–4). 434–439. doi: 10.1016/S0168-583X(00)00221-4.

[23] Fatnah, N., Azizah, D., & Cahyani, M.D. 2020. Synthesis of Chitosan from Crab's Shell Waste (Portunus pelagicus) in Mertasinga-Cirebon. 422. 370–375. doi: 10.2991/assehr.k.200323.152.

[24] Zuorro, A., Cassiani-Cassiani, D., Meza-González, D.A., Moreno-Sader, K.A., & González-Delgado, Á.D. 2020. Evaluation of shrimp waste valorization combining computer-aided simulation and numerical descriptive inherent safety technique (NuDIST). *Appl. Sci.* 10(15). 5339. doi: 10.3390/APP10155339.

[25] Kiprop, A.K., J-Coumon, M.-C., Pourtier, E., Kimutai, S., & Kirui, S. 2013. Synthesis of Humic and Fulvic Acids and their Characterization using Optical Spectroscopy (ATR-FTIR and UV-Visible). *Int. J. Appl. Sci. Technol.* 3(8). 28–35.

[26] Santoso, U.T., Umaningrum, D., Irawati, U., & Nurmasari, R. 2010. Immobilization of Humic Acid on Chitosan using Protected Cross-Linking Reaction Method and Its Application as Sorbent for Pb(II), Cd(II), AND Cr(III). *Indones. J. Chem.* 8(2). 177–183. doi: 10.22146/ijc.21620.

[27] Ren, G., Yang, L., Zhang, Z., Zhong, B., Yang, X., & Wang, X. 2017. A new green synthesis of porous magnetite nanoparticles from waste ferrous sulfate by solid-phase reduction reaction. *J. Alloys Compd.* 710. 875–879. doi: 10.1016/j.jallcom.2017.03.337.

[28] Liu, J.F., Zhao, Z.S., & Jiang, G. Bin. 2008. Coating Fe3O4 magnetic nanoparticles with humic acid for high efficient removal of heavy metals in water. *Environ. Sci. Technol.* 42(18). 6949–6954. doi: 10.1021/es800924c.

[29] Kokubo, T. 1991. Recent progress in glass-based materials for biomedical applications. *J. Ceram. Soc. Japan. Int. ed.* 99(10). 937–944.

[30] Lenders, J.J.M., Mirabello, G., & Sommerdijk, N.A.J.M. 2016. Bioinspired magnetite synthesis via solid precursor phases. *Chem. Sci.* 7(9). 5624–5634.

[31] Liu, S., Sun, J., Yu, L., Zhang, C., Bi, J., Zhu, F., Qu, M., Jiang, C., & Yang, Q. 2012. Extraction and characterization of chitin from the beetle Holotrichia parallela motschulsky. *Molecules*. 17(4). 4604–4611. doi: 10.3390/molecules17044604.

[32] Santosa, S.J. 2014. Sorption kinetics of Cd(II) species on humic acid-based sorbent. *Clean - Soil, Air, Water*. 42(6). 760–766. doi: 10.1002/clen.201200684.

[33] Rusdiarso, B., Basuki, R., & Santosa, S.J. 2016. Evaluation of Lagergren kinetics equation by using novel kinetics expression of sorption of Zn 2+ onto horse dung humic acid (HD-HA). *Indones. J. Chem.* 16(3). 338–346. doi: 10.22146/ijc.1158.

[34] Basuki, R., Ngatijo, Santosa, S.J., & Rusdiarso, B. 2018. Comparison the new kinetics equation of noncompetitive sorption Cd(II) and Zn(II) onto green sorbent horse dung humic acid (HD-HA). *Bull. Chem. React. Eng. Catal.* 13(3). 475–488. doi: 10.9767/bcrec.13.3.1774.475-488.